

## Article

# Late Mesozoic and Cenozoic Geodynamics of the Arctic Region: Implications for Abiogenic Generation of Hydrocarbons

Nickolay Sorokhtin <sup>1,2,\*</sup>, Leopold Lobkovsky <sup>1,2</sup>, Igor Semiletov <sup>2,3</sup> , Eduard Shipilov <sup>4</sup>, Sergey Nikiforov <sup>1</sup>, Nikolay Kozlov <sup>5</sup>, Natalia Shakhova <sup>2,3</sup>, Roman Ananiev <sup>1</sup>  and Dmitry Alekseev <sup>2,3,6,7</sup>

<sup>1</sup> Shirshov Institute of Oceanology, Russian Academy of Sciences, 117997 Moscow, Russia

<sup>2</sup> Institute of Natural Resources, Tomsk State University, 36 Leninsky Ave., 634050 Tomsk, Russia

<sup>3</sup> V.I. Ilyichov Pacific Oceanological Institute, Far Eastern Branch of the Russian Academy of Sciences, 43 Baltic Street, 690041 Vladivostok, Russia

<sup>4</sup> Polar Geophysical Institute, Kola Science Center, Russian Academy of Sciences Murmansk, 183010 Murmansk, Russia

<sup>5</sup> Geological Institute, Kola Science Center, Russian Academy of Sciences, 14 Fersman Street, 184209 Apatity, Russia

<sup>6</sup> Schmidt Institute of Physics of the Earth, Russian Academy of Sciences, 10, Bolshaya Gruzinskaya Str., 123242 Moscow, Russia

<sup>7</sup> Moscow Institute of Physics and Technology (MIPT), 9, Nauchny per., 141707 Dolgoprudny, Russia

\* Correspondence: nsorokhtin@ocean.ru

**Abstract:** Late Mesozoic and Cenozoic geodynamics of the Arctic region is discussed in the context of possible mechanisms which provide multistage cyclic transformations and transport of carbon through crust and mantle. Geodynamic processes control the abiogenic generation of hydrocarbons and the patterns of their localization. Possible mechanisms of abiotic hydrocarbon generation are explained in the context of carbon transport from subduction zones to rifts and serpentization of ultramafic rocks in the rifts in the case of the Laptev Sea and Gakkel Ridge areas. The carbon of shallow crust origin migrates with encapsulated fragments of marine sediments which are consumed in the Pacific subduction zone where they become destroyed and transformed by different chemical and physical processes. The resulting C-species are involved in mantle convection flows and reach the continental rifts of the Laptev Sea and the Gakkel mid-ocean ridge. Thus, the hydrocarbons formed in the crust and in the mantle acquire signatures of abiotic origin. According to the authors, the scale of manifestation of abiogenic methanogenesis in the lower parts of the lithosphere and in the upper mantle is not so wide. Numerous small (mm and fractions of the mm) particles of exogenous matter and dispersed carbon pulled into the mantle can only form a stable crustal geochemical plume that propagates in the plane of movement of convective flows. Indirectly, the scale of manifestation of this process can be judged by the volumes of degassing of hydrocarbon and carbon dioxide gases, as well as hydrogen and its compounds in the rift systems of the earth's crust, which are extremely insignificant. However, in the cold seas of the Eastern Arctic, massive emissions of bubble methane of mixed genesis were found. As shown in the literature, the range of variability of stable isotopes of carbon and <sup>14</sup>C of methane in certain areas of discharge associated with rifting demonstrates values (anomalously heavy <sup>13</sup>C, and young <sup>14</sup>C) that can be considered as examples of presumably abiogenic origin. Our work is mostly theoretical and suggests further discussion and improvement of the mechanism of formation of abiogenic hydrocarbons and the processes of their transformation.

**Keywords:** arctic geodynamics; carbon cycle; subduction zone; rift zone; abiotic hydrocarbons; abiotic methane; gas-hydrate crust–mantle transport; carbon chemistry



**Citation:** Sorokhtin, N.; Lobkovsky, L.; Semiletov, I.; Shipilov, E.; Nikiforov, S.; Kozlov, N.; Shakhova, N.; Ananiev, R.; Alekseev, D. Late Mesozoic and Cenozoic Geodynamics of the Arctic Region: Implications for Abiogenic Generation of Hydrocarbons. *Geosciences* **2023**, *13*, 68. <https://doi.org/10.3390/geosciences13030068>

Academic Editors:  
Jesus Martinez-Frias and  
Umberta Tinivella

Received: 29 January 2023  
Revised: 20 February 2023  
Accepted: 23 February 2023  
Published: 28 February 2023



**Copyright:** © 2023 by the authors. Licensee MDPI, Basel, Switzerland. This article is an open access article distributed under the terms and conditions of the Creative Commons Attribution (CC BY) license (<https://creativecommons.org/licenses/by/4.0/>).

## 1. Introduction

The Arctic is warming dramatically, with potentially catastrophic impacts on climate through rapid mobilization of the labile reservoirs of carbon sequestered in permafrost [1].

Thawing permafrost in the Arctic is the top candidate for transferring substantial amounts of carbon from land and ocean to the atmosphere on decadal-century timescales [2,3]. One possible feedback is the release of previously produced methane (CH<sub>4</sub>) preserved within seabed deposits, such as natural gas fields and coal beds, and the collapse of CH<sub>4</sub> hydrates underlying the Arctic seabed [4,5]. However, this process remains poorly understood, which creates large uncertainties in climate research related to cryosphere-climate-carbon couplings [6,7].

The Arctic Ocean, especially the East Siberian Arctic Shelf (ESAS), has been proposed as a significant source of methane that may play an increasingly important role in the future. However, the processes of formation, removal, and transport associated with such emissions have been strongly debated. Shakhova et al. [8,9] have shown that CH<sub>4</sub> concentrations in the ESAS water were anomalously high (up to 500–900 nM) compared to the values common to ocean waters. Vigorous bubbling events (1.5 to 5.7 bubbles per second) were observed at some sites [9] as well as seepages of thermogenic CH<sub>4</sub> [10,11] indicating that part of the water column supersaturation likely results from a seabed source. The destabilization of gas hydrates is frequently discussed as a CH<sub>4</sub> source in this region (e.g., [6,12–14]), but important gaps exist in the assessment of the quantity and the nature of CH<sub>4</sub> stored or formed in the Arctic seabed.

In this respect, the carbon isotope composition of CH<sub>4</sub> was analyzed on gas extracted from sediment and water samples collected at numerous locations of the shallow ESAS from 2007 to 2013. The <sup>14</sup>C content of CH<sub>4</sub> from the ESAS hotspot cores covers a range from 0.79 to 3.4 pmC corresponding to a radiocarbon age of 26 to 39 kyr BP [15], i.e., a Pleistocene age of carbon substrate. For the ID-11 non-ebullition core, <sup>14</sup>C values are unexpectedly high and vary from 87 pmC (radiocarbon age = 1 kyr BP) to 2367 pmC (Figure 2), this being a substantial enrichment above the natural background. The same applies to water samples from the shelf edge. Note that levels close to 100 pmC indicate modern values. Given that even samples affected by the nuclear bomb testing in the 1950s and 1960s show levels below 200 pmC [15], the <sup>14</sup>C >200 pmC values cannot be caused by known natural processes.

Here, we permit potential readers to focus on the discussion initiated by Sapart et al. [15] regarding hypotheses targeted at understanding such challenging data. The observation of unexpectedly high <sup>14</sup>C values for the ID-11 non-ebullition core and water samples from the shelf edge [15] needs further discussion. No naturally occurring carbonaceous material, including CH<sub>4</sub>, can surpass the <sup>14</sup>C = 200 pmC level, not even at the height of the nuclear bomb tests of the mid-20th century [15]. The <sup>14</sup>C values > 200 pmC may originate from in situ cosmogenic or nuclear production of radioactive CH<sub>4</sub> or its substrate. Enhanced <sup>14</sup>C is known from meteorites [16] and can be produced at the surface of ice sheets [17], but its amount in both cases is very small compared to what was observed in the Buor-Khaya Bay and shelf edge sediment and water samples [15]. Nuclear production of <sup>14</sup>C involves neutron activation as a consequence of a nuclear chain reaction, which may take place naturally or artificially. In the atmosphere, neutrons generated by cosmic rays can react with <sup>14</sup>N to produce <sup>14</sup>C. Evidence of a natural nuclear reactor has been found in the only place on the Earth: Oklo, Gabon [18]. However, such natural reactors can be no longer active nowadays, as the relative abundance of fissile <sup>235</sup>U has decayed below the threshold required for a sustainable reaction chain. Another explanation can be related to the fate of groundwater enriched by <sup>14</sup>C-CH<sub>4</sub>—a product of numerous nuclear bomb explosions (in the 1970s) in northern Yakutia, south of the Lena River Delta. Below, we propose to discuss additional mechanisms of abiogenic methane generation. Additional mechanisms of abiogenic methane generation may be associated with geodynamic processes.

Alternative mechanisms of abiogenic methane generation may be associated with geodynamic processes. The evolution of oceans is largely driven by interactions of crust and mantle material in rifts and continuous enrichment of the crust with many chemical compounds, including inorganic hydrocarbon gases, which accumulate on the surface and then sink to the mantle in subduction zones. Most hydrocarbon gases are generated in

rifts during serpentinization of iron-bearing ultramafic rocks by FeO to Fe<sub>2</sub>O<sub>3</sub> oxidation and CO<sub>2</sub> to CH<sub>4</sub> reduction, with the release of hydrogen due to dissociation of seawater on Fe<sup>2+</sup>. Such reactions are exothermic and can release noticeable amounts of heat, up to 180 kcal/mol at 400 °C [19–21]. A lesser portion of abiogenic hydrocarbons may originate from the transport of encapsulated C-bearing gas-fluid phases and solid C compounds by mantle convection flow from subduction zones to rifts [22,23]. Both formation mechanisms of hydrocarbon gases imply multiple changes of C-bearing material in the crust–mantle branch of the global carbon cycle.

Serpentinization of the oceanic lithosphere produces genetically pure inorganic methane and hydrogen, while more complex transformations in subduction zones and in the upper mantle lead to the conversion of organic matter into inorganic compounds. Two to nine million tons of methane are generated annually in the oceanic crust [21]. Commonly, methane and hydrogen released in hydrotherms of mid-ocean ridges dissipate in oceanic water. However, serpentinization can continue in sediments that bury rift valleys in the case of slow rifting, and the released abiogenic and biogenic hydrocarbons can form gas-hydrate deposits [24,25]. At the same time, the share of abiogenic hydrocarbons will most likely not be significant. However, the authors focus on the possible contribution of abiogenic methane, which can be associated with the existence of extremely heavy values of <sup>13</sup>C-CH<sub>4</sub> mentioned by Steibach et al. [10]. Note that the authors of this paper documented, but did not discuss the possible mechanism for the origination of the heavy tail in <sup>13</sup>C-CH<sub>4</sub>, which was found at one seepage site. Gas hydrates can further transform into oil and gas accumulations with the mediation of bacteria, whose metabolism can maintain the conversion of CH<sub>4</sub>, H<sub>2</sub>, and H<sub>2</sub>S into more complex hydrocarbons [26].

Living organisms play an important role in the transformations of carbon in crustal, atmospheric, and hydrospheric reservoirs [27–30]. Earlier data include the behavior of carbon isotopes in the global geochemical cycle [31], while recent results based on modeling and experiments for possible mantle flows and carbon reservoirs allow a hypothesis of carbon transport from the core–mantle boundary to the crust with mantle plumes, in the presence of water and oxygen [32–34].

Our previous studies on crust–mantle interactions [22] justified the presence of a deep branch of the carbon cycle without reference to carbon generation in the outer core and in the lower mantle, as well as without notable amounts of water and oxygen in the latter. Most of the carbon inputs maintaining the crust–mantle branch of the carbon cycle were hypothesized [22] to come from organic and inorganic carbonate bottom sediments which store abundant C compounds supplied, in their turn, from pelagic and terrigenous sources, including black shales shed from continental margins. The slab material consumed in subduction zones sinks into the sublithospheric mantle where it is recycled and then rises back to the surface with magma and fluids. Some compounds and monomineral fractions of carbon become encapsulated, reach the mantle depths, and are carried by the upper mantle convection flows to the zones of discharge beneath rifts, where they return to the hydrosphere as new compounds (Figure 1).

In this study, we are trying to provide grounds for the formation conditions and location of inorganic methane in the Arctic region in the context of Late Mesozoic–Cenozoic geodynamics. The revealed mechanisms of multistage transformations of carbon compounds and their conversion from organic to inorganic species and back allow considering the crust–mantle branch of the global carbon cycle as natural turnover in dry mantle conditions.

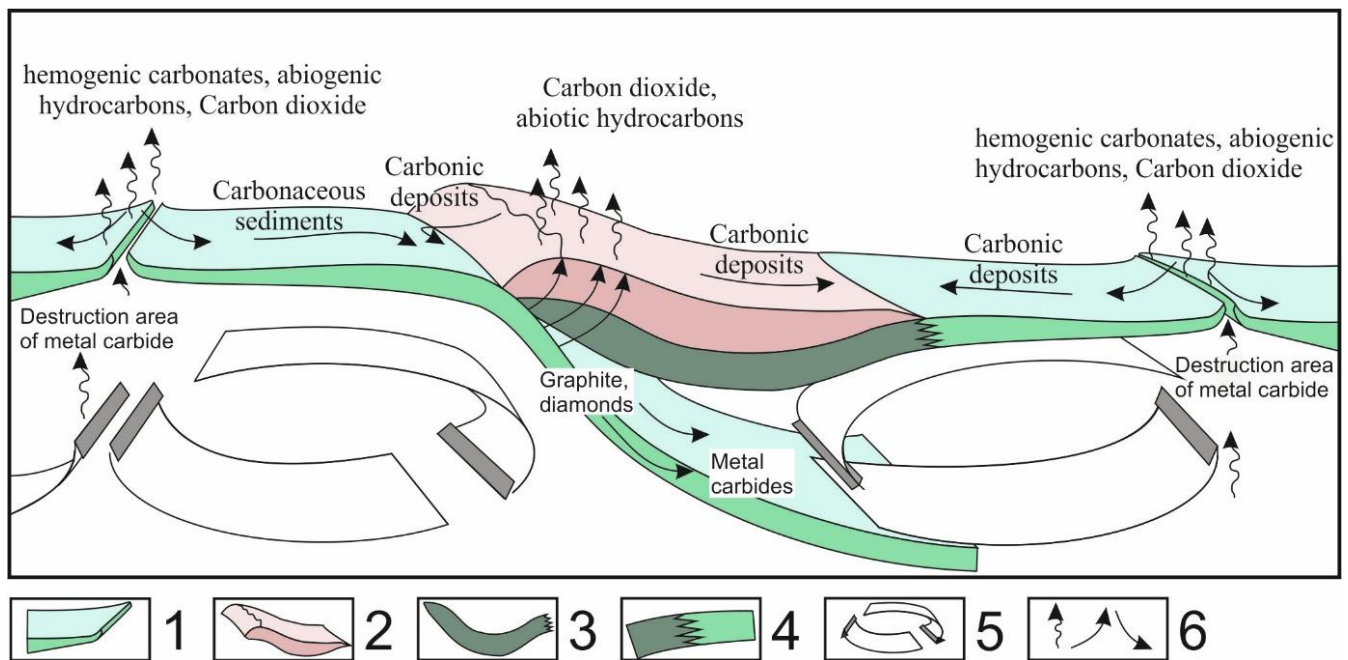


**Figure 1.** Crust–mantle carbon cycle in the ocean, modified from [22]. 1—oceanic lithosphere; 2—continental crust; 3—subcrustal continental lithosphere; 4—transition from continental to oceanic lithosphere; 5—upper mantle convection flows; 6—migration of carbon compounds.

## 2. Late Mesozoic and Cenozoic Geodynamic History of the Arctic

In recent years, in a series of studies L. Lobkovsky et al. proposed a new geodynamic model for the evolution of the Arctic lithosphere in the Late Mesozoic and Cenozoic [35–42], based on the hydrodynamic interpretation of seismic tomography data of the upper mantle in the transition zone between the northwestern part of the Pacific Ocean and Northeast Asia [43–45]. The material of this section essentially follows these studies.

Seismic tomographic images of the mantle in Northeastern and Eastern Asia, with the adjacent marginal seas of the northwestern Pacific [43–45], show cold slab material transforming into a flat layer spreading thousands of km beneath Eurasia at the lower–upper mantle transition (Figure 2). A similar geodynamic mechanism may work in the Aleutian zone of subduction to the Arctic Ocean.

In terms of fluid dynamics, such a pattern implies the presence of an upper mantle convection cell, with a horizontal branch beneath the continent along the lower–upper mantle transition and an upper branch of sublithospheric return flow toward the Pacific subduction zone, which leads to the extension of continental lithosphere, rifting, and related magmatism [35]. This interpretation of tomographic images appears more reasonable than the idea of a stagnant plate stuck in the mantle transition zone [44,45].

The slab material in the Pacific subduction zone fails to penetrate the lower mantle because of positive buoyancy produced by heat-consuming phase change at the lower–upper mantle boundary [46] but rather spreads along this boundary. The Pacific plate motion records stable mantle convection in this part of the globe as an external agent, influencing the adjacent convection region beneath the continent and continuously supplying relatively cold and heavy lithospheric material to the lower transition layer [35]. This material apparently entrains fragmented and encapsulated crustal material which sinks below the diamond stability zone and becomes dispersed by convection flows [47].

The upper mantle convection is rather unsteady, with the subcontinental convection cell being extended with ever-new material inputs, both inward on the continent and toward the Pacific Ocean. As a result, subduction zones, together with island arcs, move off the continent and form back-arc basins (Figure 3).

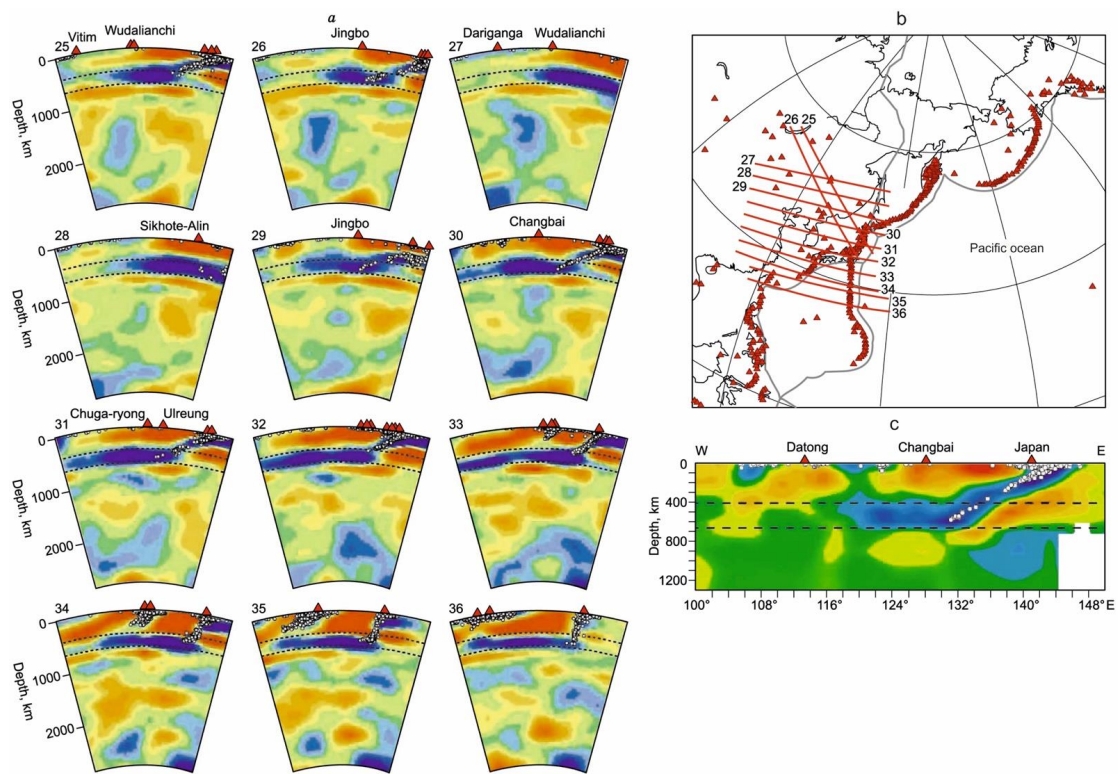


**Figure 2.** *P*-wave seismic tomography images of the mantle (a) along profiles shown in panel (b) and mantle beneath East Asia (c), modified from [37]. Red and blue colors in panels (a,c) refer to low and high seismic velocities, respectively, with maximum velocity anomalies of 1% (a) and 2% (c). White dots are earthquakes located within 100 km from the profiles; red triangles are volcanoes. Dash lines are seismic discontinuities at 410 and 670 km. Heavy lines in panel (b) are plate boundaries.

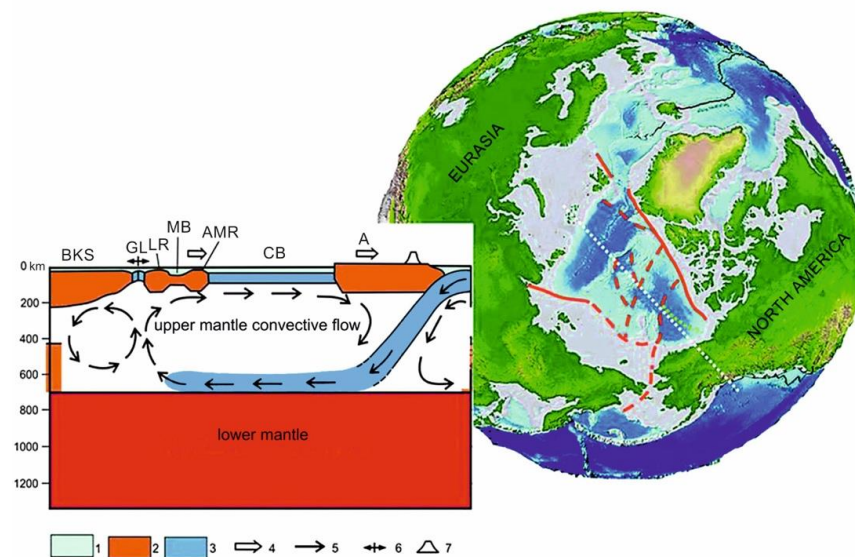


**Figure 3.** Geodynamic model of upper mantle convection associated with the Pacific subduction that explains the opening of the Eurasian Basin (left) and location of transform faults involved in the opening of the Arctic Ocean, modified from [41]. White dotted line traces the model geodynamic section. 1—sediments and water; 2—continental lithosphere; 3—oceanic lithosphere; 4—motion of Amerasian microplate; 5—upper mantle flows; 6—spreading axis in Eurasian Basin; 7—volcanism. Abbreviations stand for BKS—Barents-Kara shelf, GR—Gakkel Ridge, LR—Lomonosov Ridge, MB—Makarov Basin, AMR—Alfa-Mendelev Rise, CB—Canada Basin, A—Alaska.

This mechanism naturally explains the extension of the continental lithosphere, which is quite far from subduction or collision fronts. As confirmed by a wealth of geological and geophysical data [36,48], such processes produced regional W—E extension features in the Arctic lithosphere, from the Early Cretaceous (Aptian—Albian) and through the Cenozoic [36–39]. This hypothesis may also account for the origin of rifts in eastern and southeastern North Asia, including the Baikal rift and rifts in China, which possibly evolved over an expanding upper mantle convection cell beneath Eurasia and the Arctic region, with Pacific slab inputs (Figure 3).

The ascending mantle flow weakens the lithosphere and maintains rifting of the Alfa and Mendeleev Ridges off the Barents-Kara margin under extension and drag force produced by the cohesion of the return flow with the lithospheric base. As a result, zones of thin continental crust appear in the back of the ridges and accommodate the Makarov and Podvodnikov Basins. The rifting of the Alfa and Mendeleev Ridges off the continent, with the related opening of the Makarov and Podvodnikov Basins, occurred between 110 and 60 Ma [37–39]. During that time span, the convection cell grew horizontally on account of both the subduction zone retreat toward the Pacific Ocean and the cell front advance inward the Barents Sea margin, as slab material was supplied continuously from the subduction zone to the upper mantle convection cell. Eventually, the Lomonosov Ridge detached from the Barents Sea margin in the Cenozoic, with the Eurasian Basin formed at its back. The continental crust thus became weaker and the slow spreading produced the Amundsen and Nansen Basins separated by the Gakkel Ridge [35,37–39] (Figures 3 and 4).

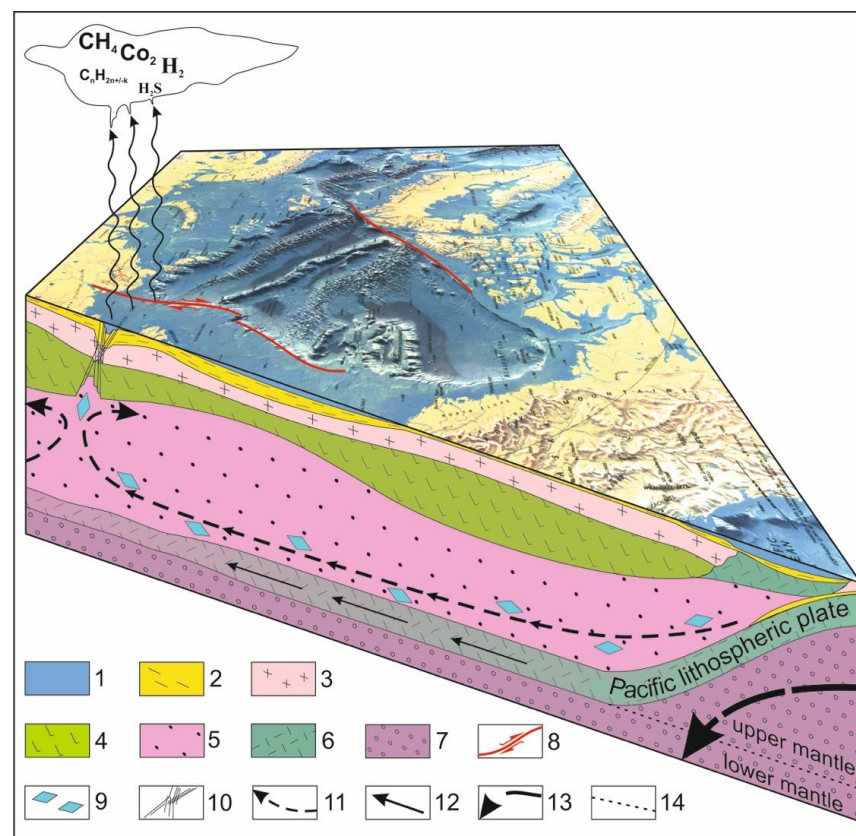


**Figure 4.** 3D geodynamic model of the Arctic Basin. 1—offshore areas; 2—sediments; 3—continental crust; 4—subcrustal lithosphere; 5—asthenosphere; 6—slab (color grades show the degree of deformation and heating); 7—upper mantle; 8—Spitsbergen-North Greenland and Khatanga-Lomonosov transform faults; 9—encapsulated C compounds consumed in subduction zone; 10—continental rift; 11—mantle convection flow; 12—slab motion; 13—large-scale mantle convection; 14—lower-upper mantle boundary.

The opening Arctic Ocean in the Late Mesozoic–Cenozoic was limited by two large transform faults: the Spitsbergen–North Greenland zone from the Canadian side and the Khatanga–Lomonosov zone from the side of Russia. As the Eurasian Basin was opening, the Lomonosov Ridge was part of the newly formed Amerasian plate [40,41,49–51] and underwent right-lateral strike-slip motion on the Khatanga–Lomonosov fault zone (KL transform). In this model, the zone of faults makes a kind of geodynamic boundary between the Amerasian microplate and Eurasia, while the Lomonosov Ridge and the Amundsen Basin (part of the Eurasian Basin) form a kinematic couple [41,42].

The Khatanga–Lomonosov zone of transform faults, like the Spitsbergen–North Greenland one, is a transregional feature which encompasses both oceanic and continental lithosphere. The transform faulting is an intrinsic element of lithospheric processes related to the upper mantle convection [40,41] (Figures 3 and 4) which is indispensable to explaining the origin of the Makarov [52], Norwegian–Greenland [50,51,53], etc., Eurasian [54], and other spreading basins. The formation of spreading basins and the related processes in the lithosphere appear to be driven by the motion of sublithospheric material in the upper mantle convection flow toward the Aleutian subduction zone. This motion causes drag and creep of the lithosphere accompanied by extension in some places and compression in other places of the same plate [35]. In this case, it was the composite Amerasian microplate which moved toward the Pacific subduction zone along roughly parallel transform faults on the Arctic Canada and Siberian–Chukchi shelves [41,42] (Figure 4). The Amerasian microplate comprised Alaska, Canada Basin, Chukchi Rise, Alfa–Mendeleev Rise, Podvodnikov and Makarov Basins, and Lomonosov Ridge.

The intersection of the Khatanga–Lomonosov transform zone and the Gakkel Ridge on the Laptev shelf is marked by a zone of extension with a thin continental crust [42,55]. Interpretation of seismic time sections (Figure 5) revealed serpentinized mantle rocks in contact with Late Cretaceous–Late Eocene water-saturated sedimentary complexes [56]. Therefore, ultramafic mantle rocks in the Ust’-Lena continental rift are flushed with meteoric waters, which lead to their serpentinization, as in the case of the Gakkel Ridge.

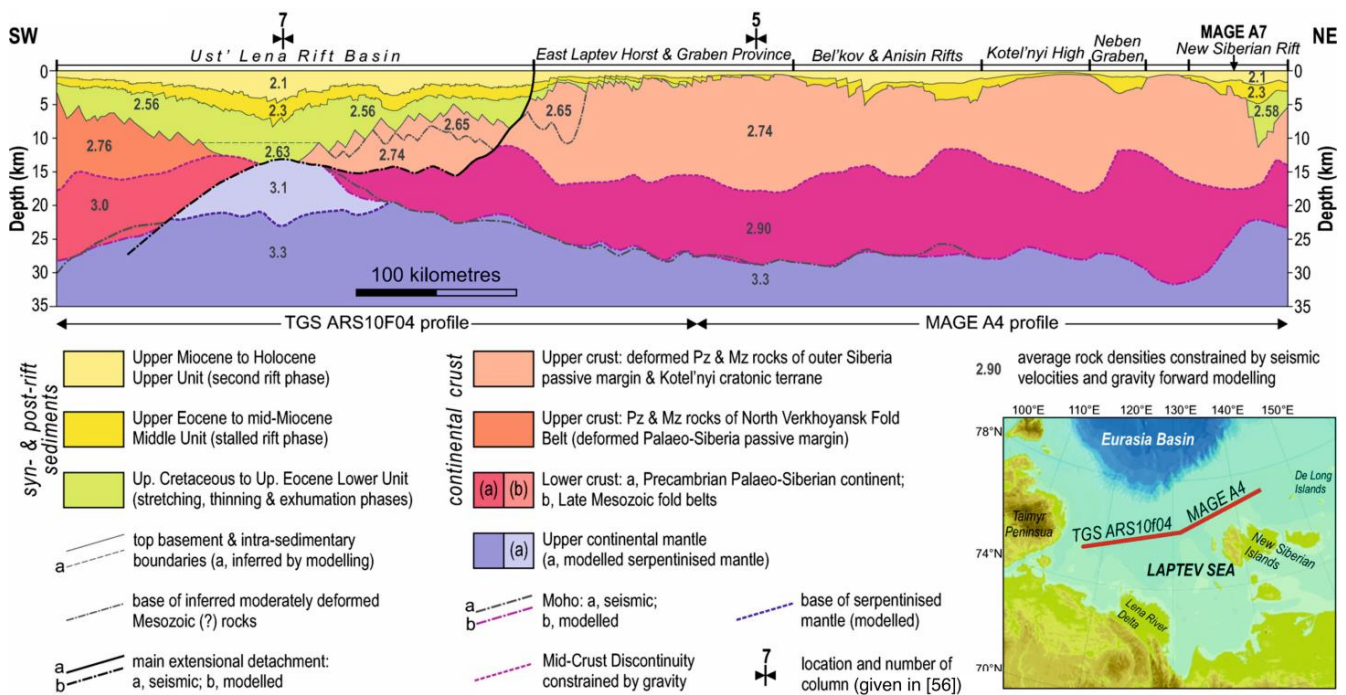


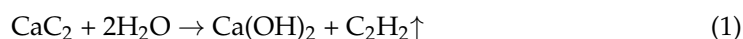
Figure 5. The gravity model of the crust in the Laptev shelf along the transect, modified from [56].

### 3. Origin of Abiotic Methane, Other Hydrocarbon Gases, CO<sub>2</sub>, and H<sub>2</sub> in Rift Zones

The fractured rifted crust in zones of seafloor spreading conduits of basaltic melts rising from the mantle depths. The oceanic lithosphere under a thick layer of water becomes hydrated and a serpentinite layer is formed in its lower part by the crystallization of olivine-bearing ultramafic material. Seawater can percolate to a depth limited by overburden pressures of ~2.3 kbar where serpentinite becomes ductile and heals fractures [21]. Hydrous oceanic lithosphere above this depth contains at least 5 wt.% of water bound in hydrosilicates and especially in serpentinite containing no less than 10–11 wt.% H<sub>2</sub>O.

The hydrothermal systems of mid-ocean ridges carry to the hydrosphere enormous amounts of material generated in the oceanic lithosphere and upper mantle, including silica, calcium, magnesium, manganese, metal sulfides, methane, carbonates, sulfates, and many other compounds [57,58]. However, diverse and voluminous hydrocarbons known from oceanic hydrothermal fields (e.g., CH<sub>4</sub>, C<sub>2</sub>H<sub>6</sub>, C<sub>3</sub>H<sub>8</sub>, C<sub>4</sub>H<sub>10</sub>, C<sub>6</sub>H<sub>6</sub>, and C<sub>7</sub>H<sub>8</sub> coexisting with H<sub>2</sub>O and CO<sub>2</sub> at the northern border of the Juan de Fuca Ridge in the Pacific Ocean [59] or CH<sub>4</sub>, C<sub>2</sub>H<sub>6</sub>, C<sub>2</sub>H<sub>4</sub>, C<sub>3</sub>H<sub>8</sub>, and C<sub>4</sub>H<sub>10</sub> in the Mid-Atlantic ridge [60]) hardly can come from the mantle but rather appear to result from the decomposition of crustal rocks or from an alteration in mantle-derived material at shallow depths. The presence of carbon compounds in rifts may be due either to the transport of dispersed encapsulated fragments of crustal material and monomineral phases by mantle convection flow from subduction zones, or to hydration and serpentinization of the lithospheric mantle. It is reasonable to expect that carbon at the depths of convective mantle mixing, which is below the diamond stability limit, exists as metal carbides or is present in encapsulated supercritical fluids of magmatic-hydrothermal systems.

Metal carbides, solid particles of crustal material, and gas-fluid inclusions migrating from subduction zones to rift regions above mantle convection flow (Figure 1) reach the hydration depths (Figure 6) where metal carbides easily decompose to release hydrocarbons and metal hydroxides within the zone of fluid stability. Importantly, the melting point of many metal carbides ranges from 1000 °C to 4000 °C and is often much higher than the upper mantle temperature (~1300 °C to 1600 °C). Therefore, metal carbides can be stable in an almost dry mantle and retain their crustal geochemical signatures. For example, Ca and Na carbides rising to shallow depths in rifts decompose with the formation of acetylene [61]:



Carbides of Na, K, and some other metals decompose by the same reactions. In the presence of metals, acetylene becomes hydrated and can convert into ethane in two steps:



Note that the hydrolysis reaction of alkali metal carbides can be extremely rapid and explosive under normal conditions, in the presence of large water volumes, but is slow in geological systems on the scale of millions of years, under subsolidus temperatures, pressures of a few kbar and at minor amounts of free water.

Hydration of Al and Mn carbides releases methane:



The hydration reactions with BeC<sub>2</sub> and Li<sub>2</sub>C<sub>2</sub> occur in the same way. Mn(OH)<sub>2</sub> produced by reaction (5) oxidizes easily in the presence of dissolved oxygen, with the formation of pyrolusite:



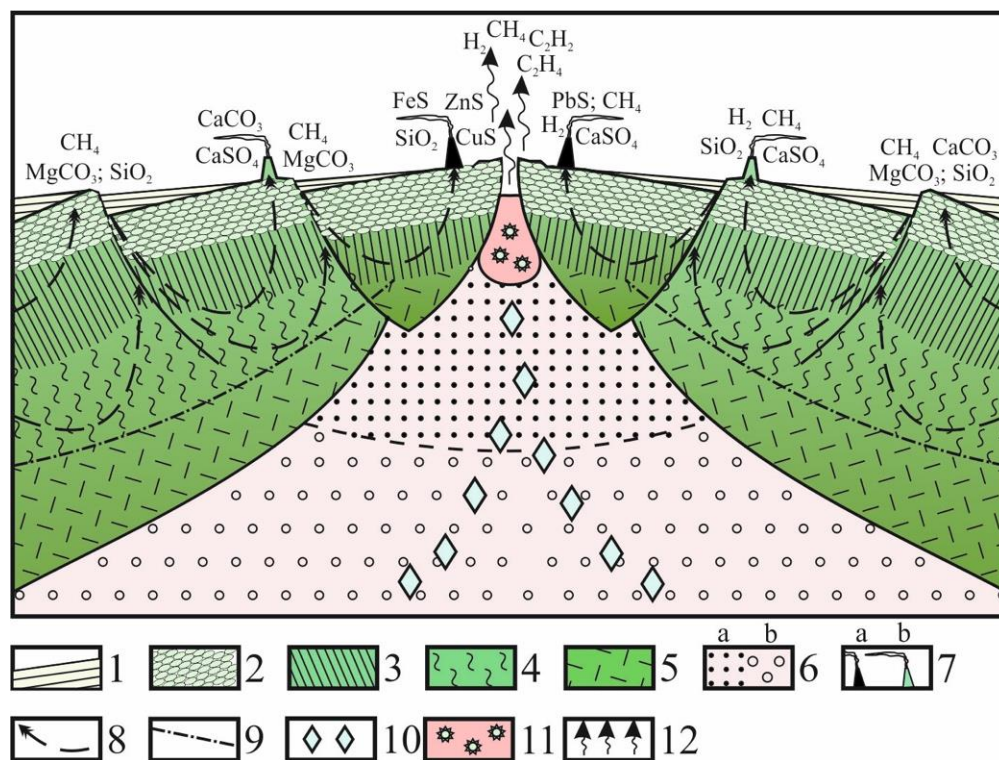
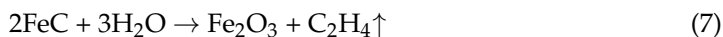
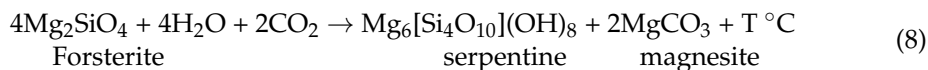


**Figure 6.** Chemistry of hydrothermal processes and generation of carbon compounds in mid-ocean rift zones, modified from [22,47]. 1—sediments; 2—basalts (pillow lavas); 3—dolerite dikes (dike-in-dike complexes); 4—serpentinite layer; 5—subcrustal lithosphere; 6—magma source under ridge crest (a) and asthenosphere (b); 7—vents at black (a) and white (b) smokers; 8—seawater flows in oceanic crust; 9—critical water stability level; 10—metal carbides, encapsulated solids, and gas-fluid inclusions in dehydrated sediments transported from subduction zones; 11—decomposition of metal carbides; 12—outgassing products of metal carbide decomposition.

The decomposition of iron carbides is accompanied by C<sub>2</sub>H<sub>4</sub> release but is likely of limited natural occurrence because most iron tends to sink into the lower mantle and only minor amounts of carbides can subsequently reach oceanic rifts. Nevertheless,



Hydration of shallow mantle in rifts leads to the crystallization of mafic and ultramafic rocks and produces carbonate and silicate compounds that migrate from deep oceanic crust and are deposited on the seafloor. All reactions are irreversible and heat-releasing. The hydration of olivine-bearing crustal rocks that binds CO<sub>2</sub> and yields chemogenic carbonates is among key reactions of this kind:



The resulting continuous inputs of material to the ocean maintain the life of skeletal organisms (corals, mollusks, foraminifera, coccolithophores, etc.) which transform dissolved inorganic carbonates into organic species.

Hydration of olivine in rifts in the presence of carbon dioxide leads to the generation of abiotic methane by iron oxidation:



sink and eventually become assimilated by the mantle, whereas fluids and carbonate and silicate melts, which cannot ascend, stack near the plate base and form sources of ultramafic alkaline, carbonatite, and lamproite–kimberlite magmas or partly migrate to rifts with convection flows (Figure 8).

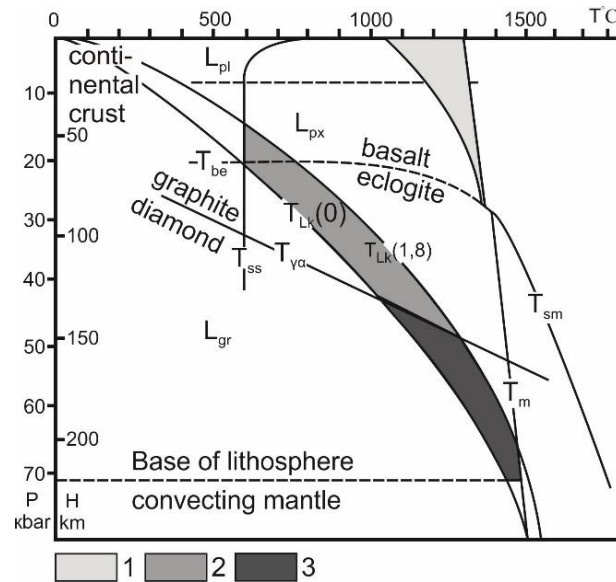


**Figure 7.** Thermodynamic melting conditions for ultramafic alkaline and kimberlite magmas [64]. 1—domain of juvenile basaltic melts; 2—domain of ultramafic alkaline and carbonatite melts; 3—domain of diamondiferous lamproite, kimberlite, and carbonatite melts;  $T_m$ —mantle temperature;  $T_{sm}$ —mantle solidus;  $T_{be}$ —temperature of basalt-to-eclogite conversion;  $T_{\gamma\alpha}$ —temperature of graphite-to-diamond conversion;  $T_{LK}(0)$ —modern continental geotherm;  $T_{LK}(1,8)$ —continental geotherm at 1.8 Ga;  $L_{pl}$ ,  $L_{px}$  and  $L_{gr}$ —stability fields of plagioclase, pyroxene, and garnet lherzolite;  $T_{ss}$ —melting point of water-saturated sediments.

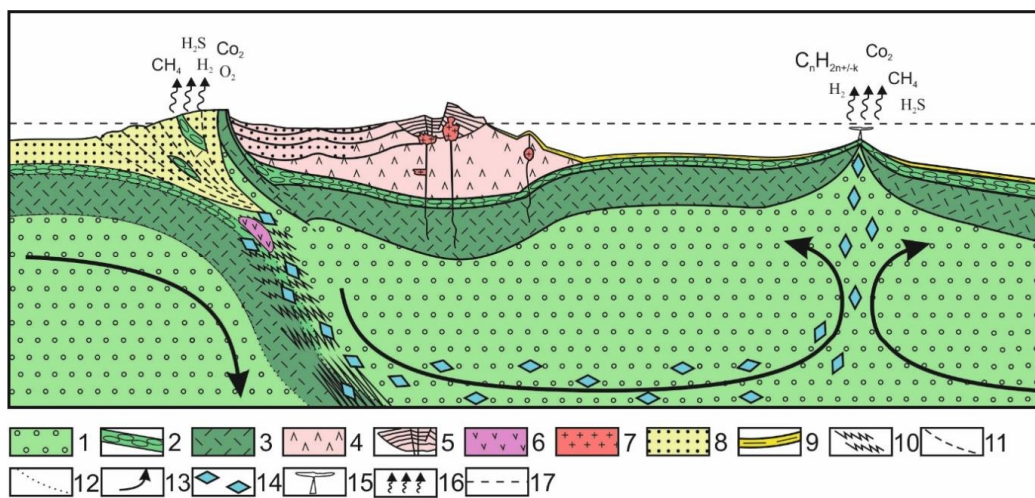


**Figure 8.** Generation of abiogenic hydrocarbons at convergent and divergent plate boundaries. 1—asthenosphere; 2—oceanic crust; 3—oceanic lithosphere (crystalline upper mantle); 4— island arc complexes; 5—caldera-type volcanic-sedimentary complexes; 6—sources of carbonatite and kimberlite magmas; 7—granitoid intrusions; 8, 9—sedimentary complexes: undifferentiated marine and island arc (8) and marine (9) sediments; 10—zone of dynamic metamorphism, peak phase; 11—large faults; 12—partial slab disintegration; 13—mantle convection flows; 14—encapsulated solid and gas-fluid inclusions derived from crustal material; 15—hydrothermal systems; 16—outgassing compounds; 17—water surface.

The transition zone between the continental lithosphere and the convecting mantle is free from notable temperature or density variations, at similar chemical parameters, and rather corresponds to the brittle-to-ductile transition. Slab dehydration in this zone is incomplete, and the remaining portions of water, carbon, C compounds, CO<sub>2</sub>, and some other volatiles can sink into the mantle.

Consumption of C-bearing compounds in subduction zones leads to their multistage transformation and release of monomineral carbon. Graphite converts to diamond at depths of approximately 120–150 km, which is the depth range of diamond crystallization and formation of typical diamond-pyrope mineral assemblages in eclogites and garnet peridotites [65]. On the other hand, rhombic olivine converts to a denser spinel phase (ringwoodite) about 350 km [66], and its absence from natural kimberlites or diamond inclusions [67] means that the original depth of diamond-bearing rocks must be limited to 300 km (Figure 7). Taken together, these data place constraints on the equilibrium range of diamond-bearing eclogites and garnet lherzolites [65,67,68]: 1120–1380 °C and 1300–1500 °C, respectively, at pressures of 50 kbar and 70 kbar; for garnet lherzolites, the range is from 900 to 1400 °C (Figure 7).

Thus, carbon may convert back to graphite at depths below 250–300 km, in the stability field of metal carbides, and makes up various compounds with the latter. Carbide mineral species are known from quite a few natural occurrences (meteorites, kimberlites, metamorphic ultramafic rocks, and shungites) because they originate at large depths but are prone to decomposition at low pressures and temperatures in the presence of water. They are, namely, cohenite (Fe,Ni,Co)<sub>3</sub>C, moissanite (SiC), tantalcarbide (Ta,Nb)C, niobocarbide (Nb,Ta)C, khamrabaevite (Ti,V,Fe)C, as well as vanadium (V<sub>8</sub>C<sub>7</sub> and V<sub>2</sub>C) and chromium (Cr<sub>2</sub>C<sub>3</sub>) phases. Metal carbide phases, including carbides of Ca, Al, Mn, Fe, and some other metals, may be more abundant in the upper mantle. The reactions in subduction zones are irreversible, heat-releasing, or heat-consuming, and occur in different redox conditions. The related processes develop through geological time and eventually bring all system parameters to the thermodynamic equilibrium.

Modern marine sediments store 20–40 wt. % of water, while their diagenetically altered varieties are less hydrous (10–15 wt.% H<sub>2</sub>O). The hydrous phases in pelitic sediments include illite, smectite, montmorillonite, kaoline, and diaspore, which also contain 0.5 to 1.0 wt.% OM. However, slab sediments in subduction zones undergo intense dehydration early during metamorphism and lose first free water from pores and then bound water from the crystal structure. Afterwards, the sedimentary material undergoes further alteration by heat-consuming reactions, with the ensuing release of water, CO<sub>2</sub>, silica, alkalis (especially, potassium), and lithophile elements. The dehydrated rocks in zones of maximum compression become denser and partly seal the forming solutions, thus increasing the fluid pressure and extending the stability fields of hydrous minerals.

Most of these formed fluids flow upward and orthogonally to the long axis of arcs (margins) from the regions of high pressure to zones of tectonic shadow, being driven by a shear pressure gradient. The fluids move across transition zones between metamorphic facies (Figure 9), where minerals crystalize at the boundaries of the respective stability fields. The model of Figure 9 has another important geodynamic implication: at large depths in subduction zones, the plate contacts become less distinct and the mineral assemblages are in thermodynamic equilibrium, while the fluid phase acquires features of a supercritical fluid. This effect is primarily due to the compositional proximity of material in the third layer of oceanic and continental lithosphere, whereby the slab sinking into the mantle together with remnant sediments becomes confined between similar mantle complexes.

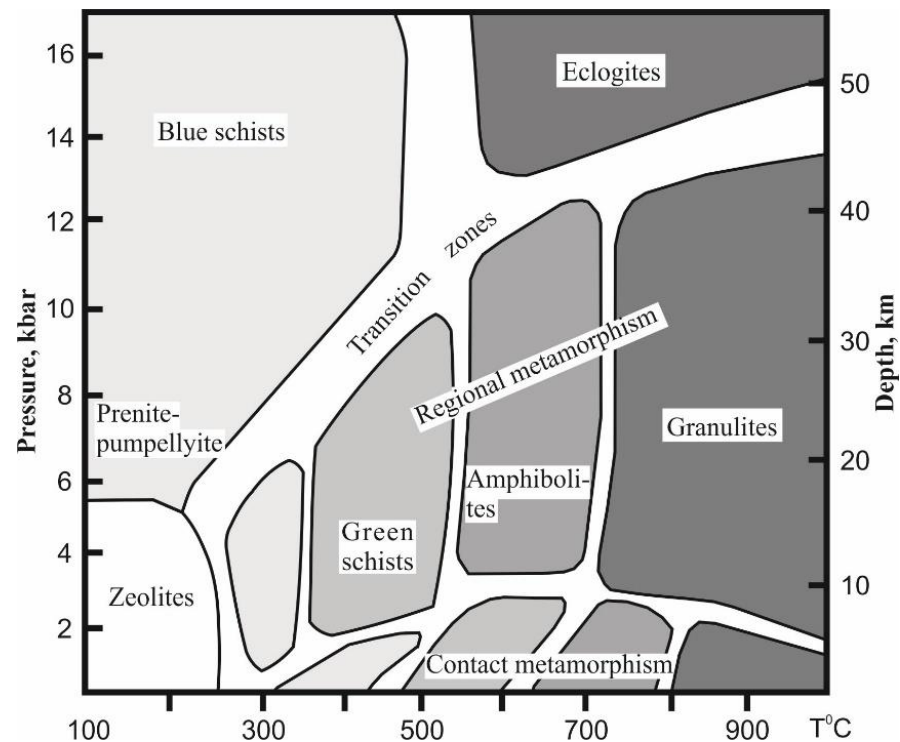
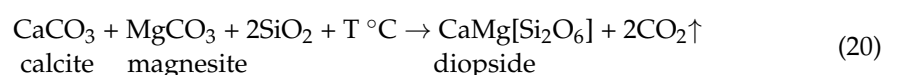
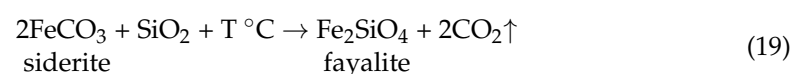
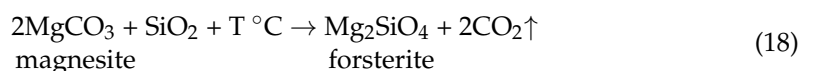
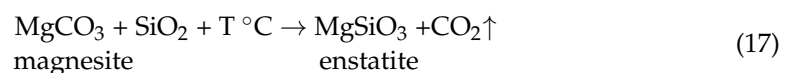
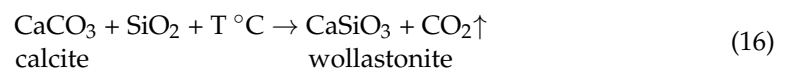


Figure 9. Metamorphic facies in  $P$ - $T$  coordinates, modified from [69].

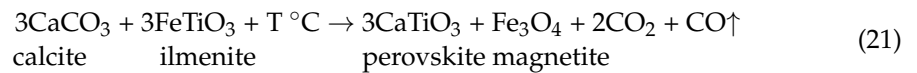
This process inevitably leads to the separation and isolation of different volumes of material, encapsulation of crustal melts, metamorphic crustal rocks, disseminated material, fluids, and gas-fluid inclusions. The gas-fluid inclusions in the sublithospheric mantle turn into a supercritical fluid, without distinction between the two components. The capsules are transported to the convecting mantle in the conditions of viscous flow, detach from the slab or move together with it into the ascending convection branch, and are dispersed over long distances (Figures 4 and 8).

Prograde dynamic metamorphism induces the formation of hydrothermal fluids in heating water-saturated rock systems. Carbonates that fall into subduction zones are subject to alteration and break down with the release of  $\text{CO}_2$ , whereby bases become bound either in silicate phases or in carbonates. Minerals can form out of the constituent oxides if heat is available: 22.3 kcal/mol for siderite, 23 kcal/mol for magnesite, and 42.6 kcal/mol for calcite [62]. Thus, dissociation of carbonates is possible by heat-consuming reactions in hot regions of subduction zones, at depths of 80–100 km for siderite and magnesite and below 150 km for calcite, i.e., in the melting region of water-saturated sediments.



Carbon dioxide released in reactions (16)–(20) dissolves in the formed melts and enters the H<sub>2</sub>O-CO<sub>2</sub> fluid.

Decomposition of carbonates under high pressures of 40–50 kbar in continental lithosphere must be accompanied by iron oxidation, producing dense crystalline structures of magnetite and reducing CO<sub>2</sub> to CO:



Garnet, corundum, and calcite are formed at still greater depths, with CO<sub>2</sub> release:



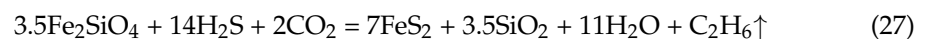
In addition to (21)–(23), reactions at still higher temperatures and pressures may lead to the decomposition of carbonates in the presence of olivine or pyroxene, with the release of free carbon dioxide and formation of monticellite and periclase:



In the presence of CO<sub>2</sub> and H<sub>2</sub>S, olivine (fayalite) can decompose to marcasite (FeS<sub>2</sub>), magnetite (Fe<sub>3</sub>O<sub>4</sub>), quartz, water, and abiogenic methane [59]:



and even heavier hydrocarbons, such as ethane:



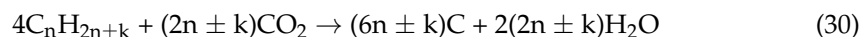
Diamonds are formed deeper than 120–150 km by carbon reduction, via reactions of CO<sub>2</sub> and CO with methane or other organic or inorganic hydrocarbons involved in subduction zones together with sediments. Marine sediments and clastics shed from continental margins often bear large amounts of organic matter, which undergoes thermolysis and hydrolysis in subduction zones and rapidly converts into hydrocarbons, nitrates, and ammonia compounds in several short stages. Some of the mobile compounds become squeezed out, together with pore waters, to shallow levels of subduction zones, but some descend further into the mantle with clastic material. In modern subduction zones, where hydrous silicate melts easily leave the zones of friction between plates, magma generation temperatures rise rapidly until the melting point of basalt. Therefore, most carbon-bearing compounds fail to penetrate deep into the mantle because they almost completely dissociate with the formation of disseminated graphite long before.

At high temperatures and pressures, hydrocarbons lose stability and undergo cracking (breakdown of carbon bonds in large hydrocarbon molecules) [70] whereby complex hydrocarbons become fewer while simple compounds increase in abundance. Since methane is the most stable and tolerates temperatures up to 1200 °C (at atmospheric pressure), all organic matter can eventually transform into methane, hydrogen, and free carbon in high-pressure, high-temperature conditions. Note that carbon released by the thermal destruction of hydrocarbons remains disseminated as no crystalline carbon can form in the heat-consuming process. The formation of crystalline carbon occurs in heat-releasing

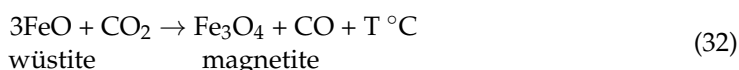
reactions that decrease the internal energy of the system, such as reactions of hydrocarbons with CO and CO<sub>2</sub> [71]:



In the general case, a diamond can form by reactions of hydrocarbons with C oxides [71,72]:



Carbon dioxide is presumably released by the thermal dissociation of carbonates (heat-consuming reactions (16)–(20)) in hot regions of subduction zones, while carbon oxide may be generated by a heat-releasing reaction, e.g., by oxidation of wüstite to the magnetite stoichiometry:



In addition to organic hydrocarbons, diamond formation may involve abiotic methane, e.g., that formed by reaction (10). Such reactions become possible due to multistage dehydration and hydration in subduction zones.

Monomineral carbon can result from a reaction to carbon dioxide with liberated hydrogen:



Reactions (28)–(31) and (33) are heat-releasing and thus can lead to crystallization of carbon in the form of graphite (at moderate pressure), diamond (at high pressures) or again produce disseminated graphite (in supercritical upper mantle conditions).

The amount of released heat under normal *P-T* conditions estimated from the enthalpy of compounds [73] is 24.6 kcal/mol in reaction (28) when methane reacts with carbon dioxide and as much as 65.9 kcal/mol in the case of reactions with CO (29). The proportion may be slightly different at higher pressures and temperatures, but the enthalpy  $\Delta H_t^0$  is always lower in reactions with CO<sub>2</sub> than with CO (since  $\Delta H_t^0 < 0$ ). Therefore, the crystallization of carbon from a CO + CO<sub>2</sub> mixture is expected to first involve CO and then CO<sub>2</sub>.

Free carbon may also form by reactions with sulfur or nitrogen compounds. Reactions with sulfur are possible as diamonds often enclose sulfides, especially pyrrhotite:



or



Note, however, that reactions (32)–(34) are heat-consuming and can only produce disseminated carbon. Nitrogen is commonly abundant in hydrothermal systems:

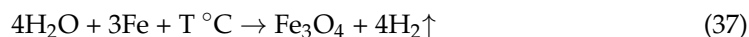


At high temperatures, NH<sub>3</sub> is unstable and apparently dissociates into nitrogen and hydrogen which then become dissolved in the fluid phase.

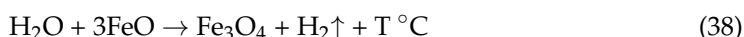
In addition to organic hydrocarbons, lower hydrocarbons of inorganic origin (i.e., methane) may be present in kimberlites, eclogites, and garnet peridotites derived from the oceanic crust. Originally, they are formed at the expense of organic material but become inorganic in a certain respect after some physical and chemical transformations, whereby

the difference between the biogenic and abiogenic origin of hydrocarbons vanishes. Most abiotic hydrocarbons in subduction zones are formed from shallow crustal material.

The generation of methane requires considerable amounts of hydrogen which may release upon dissociation of water on iron, in the heat-consuming reaction with the participation of an aqueous fluid:

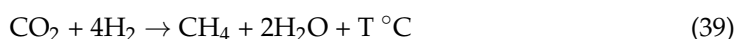


On the contrary, the reaction may be heat-releasing due to the oxidation of silicate iron to the magnetite stoichiometry:



The heat-releasing reaction is preferable, i.e., free hydrogen in diamond formation regions more likely originates in this way. Note that magnetite is a spinel phase of iron oxides and is thus the most stable under high pressures. This mechanism may account for magnetite rims around olivines and other ferrous silicates.

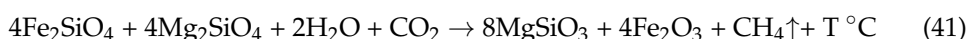
Methane is formed by simple heat-releasing reactions of CO and CO<sub>2</sub> with hydrogen or water. These reactions may accelerate and start already at 250–400 °C in the presence of catalyzing nickel, nickel carbonate, or metallic iron, but can be expected to go without catalysts at higher *P-T* conditions common to subduction zones:



In the case of 400–500 °C greenschist and epidote-amphibolite metamorphism, synthesis of abiotic methane is possible by serpentinization of iron-bearing olivine in the presence of carbon dioxide:



At higher temperatures of >660–700 °C, this reaction accompanies the formation of metasomatic pyroxene (clinoenstatite):



Moreover, abiotic methane can be generated by the oxidation of metallic iron in the presence of carbon dioxide:



In the context of methane-releasing reactions, note that carbon isotopes can fractionate easily between CH<sub>4</sub> and CO<sub>2</sub>, and <sup>12</sup>C is mostly present in both organic and inorganic methane.

According to experimental results [74,75], higher hydrocarbons (up to C<sub>10</sub>H<sub>22</sub>) can be produced by reactions with solid iron oxide, marble, and water which are possible at 1500 °C and >30 kbar (>100 km).

The discussed reactions and some other exchange reactions of carbon and hydrous compounds should produce a compositionally complex fluid phase of kimberlite melts and gas-fluid inclusions. The gas-fluid inclusions in a diamond are of special interest in this respect as they store a record of source fluid compositions. They contain 10 to 60 wt.% H<sub>2</sub>O, 2 to 50 wt.% H<sub>2</sub>, 1 to 12 wt.% CH<sub>4</sub>, 2 to 20 wt.% CO<sub>2</sub>, 0 to 45 wt.% CO, 2 to 38 wt.% N<sub>2</sub>, and ~0.5–1.2 wt.% Ar [76], as well as about 0.5 wt.% ethylene (C<sub>2</sub>H<sub>4</sub>) and 0.05 to 3 wt.% C<sub>2</sub>H<sub>5</sub>OH alcohol, but no free oxygen. The composition of gases provides unambiguous evidence that the fluid phase involved in the crystallization of diamond was

mainly of shallow origin, while the absence of free oxygen indicates reducing conditions of diamond formation.

In addition to gas-fluid inclusions, many diamonds enclose mantle-derived minerals, mostly sulfides, as well as olivine, serpentine, phlogopite, omphacite, pyrope, almandine, magnetite, wüstite, metallic iron, chromite, etc., almost all being high-pressure eclogitic or peridotitic phases.

At depths of 250 to 300 km and deeper, beyond the kimberlite magma sources, some portion of carbon and its species in gas-fluid inclusions and in monomineral diamond ( $\sim 4 \text{ g/cm}^3$  density) can sink or become consumed by the slab in the hot subsolidus upper mantle. The free carbon and its species are spread by convecting mantle flows at sublithospheric levels. Diamond in this region ( $>250 \text{ km}$  depths) converts back to graphite and binds with metals to form metal carbides which are then transported to rifts (Figure 8).

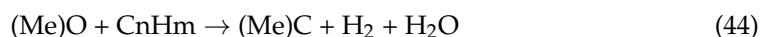
Carbon and some encapsulated solid or gas-fluid inclusions from degraded sedimentary complexes fail to make large accumulations but rather occur as a train of numerous fine particles (fractions of mm to mm) rising from the mantle to crustal levels in the plane of convective flows.

At depths of approximately 200–300 km, carbon can react with hydrogen (reactions (37) and (38)) as [77]:



where  $n$  and  $m$  are constants.

This reaction may be responsible for the presence of fluid inclusions composed of higher hydrocarbons than alcohols. Then, the reaction products react with metal oxides with the formation of carbides:

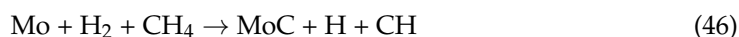


(Me stands for metal).

Carbon can reduce metal oxides with the formation of carbides in oxygen-deficient settings [78]:



For instance, Mo carbide is formed in the presence of methane and hydrogen at 700–800 °C [79]:



Li carbide can originate in a similar temperature range by fusion with calcite which is largely available in slabs (reactions (22) and (23)) [61]:



At temperatures above 900 °C, carbon reacting with iron makes a solid solution with the formation of iron carbides  $\text{Fe}_3\text{C}$  and  $\text{Fe}_2\text{C}$ :



In the presence of carbon, iron in mantle-derived rocks reduces to form a carbide phase. The formation of cohenite  $(\text{FeNiCo})_3\text{C}$  is possible under these conditions as well.

## 5. Carbon Isotope Composition in Subduction Zones and Upper Mantle

The carbon species involved in various reactions originally come from shallow sediments (see above) and their C isotope composition is controlled by the composition of reaction agents. The C isotope system in rifts and subduction zones has its own features. It is reasonable to describe isotope geochemical transformations of carbon successively from convergent to divergent plate boundaries.

The isotope composition of diamond carbon ( $\delta^{13}\text{C}_{\text{diam}}$ ) produced from abiotic methane ( $\text{C}_{\text{met}}$ ) and carbonate carbon ( $\text{C}_{\text{carb}}$ ) in subduction zones (reactions (28) and (29)) is given by

$$\delta^{13}\text{C}_{\text{diam}} = \frac{\delta^{13}\text{C}_{\text{met}} + \delta^{13}\text{C}_{\text{carb}}}{2} \quad (49)$$

$$\delta^{13}\text{C}_{\text{diam}} = \frac{\delta^{13}\text{C}_{\text{met}} + 2 \cdot \delta^{13}\text{C}_{\text{carb}}}{3} \quad (50)$$

The  $\delta^{13}\text{C}_{\text{dm}}$  values of carbon produced with the participation of  $\text{C}_n\text{H}_{2n\pm k}$  hydrocarbons and organic ( $\text{C}_{\text{org}}$ ) carbon (reactions (30) and (31)) are obtained as

$$\delta^{13}\text{C}_{\text{diam}} = \frac{4n \cdot \delta^{13}\text{C}_{\text{org}} + (2n \pm k) \cdot \delta^{13}\text{C}_{\text{carb}}}{6n \pm k} \quad (51)$$

The C isotope compositions of diamond and carbonate varieties are assumed to be roughly equal in the case of diamond formation by reaction (33):

$$\delta^{13}\text{C}_{\text{dm}} \approx \delta^{13}\text{C}_{\text{carb}} \quad (52)$$

The  $\delta^{13}\text{C}$  values of abiotic methane formed in mid-ocean ridges are about 13–14‰ [20] and those of organic carbon are most often  $\delta^{13}\text{C}_{\text{org}} \approx -15$  to  $-50$ ‰ (25‰ on average) [80]. Therefore,  $\delta^{13}\text{C}_{\text{dm}} \approx -6$ ‰, according to equation (49), at average  $\delta^{13}\text{C}_{\text{met}} \approx -25$ ‰; the range is from +0.3‰ to  $-6.3$ ‰ according to equation 50 [21].

The theoretical estimates of  $\delta^{13}\text{C}_{\text{dm}}$  generally agree with the available experimental evidence. For instance, layer-by-layer analysis of C isotope ratios in individual diamond crystals [81] showed rimward changes of  $\delta^{13}\text{C}_{\text{dm}}$ , with higher  $^{12}\text{C}$  in the cores and greater  $^{13}\text{C}$  enrichment in the rims:  $-11.01$ ‰ (core) to  $-7.32$ ‰, with a shift about 4‰. Therefore, crystal growth begins mainly at the account of organic carbon and then involves inorganic carbon with greater  $^{13}\text{C}$  contents as the slab sinks deeper into subduction zones. Thus, most diamond crystals grow from a mixture of organic and inorganic methane and decomposition products of various carbonates.

The  $\delta^{13}\text{C}_{\text{dm}}$  values were found [82] to have different patterns depending on host lithology: the patterns described above are typical of kimberlitic and eclogitic diamonds while peridotitic diamond has relatively narrow  $\delta^{13}\text{C}_{\text{dm}}$  ranges of  $-2$  to  $-8$ ‰ ( $-6$ ‰ on average). The reason may be that the formation of kimberlitic and eclogitic diamonds involves crustal carbon from shallow sources containing organic carbonates and hydrocarbons, which can account for the large  $\delta^{13}\text{C}_{\text{dm}}$  ranges. Unlike these, peridotitic diamonds could receive carbon only from chemogenic carbonates that formed during hydration of the former oceanic crust (reactions (8) and (9)) and chemogenic methane (reaction (10)).

All carbon in rifts is either transported by upper mantle convection flows from subduction zones or is generated by the hydration of mafic and ultramafic slab rocks (see above). The C isotope composition of disseminated carbon, metal carbides, and encapsulated crust fragments transported from subduction zones bears signatures of their original geodynamic environment. Thus, the carbon isotope patterns common to rift settings bear overprints of material formed in situ by slab hydration in subduction zones.

The C isotope composition of methane venting in rifts (black smokers), with  $\delta^{13}\text{C}$  about  $-13$  to  $-14$ ‰ differs markedly from average  $\delta^{13}\text{C}$  of seawater  $\text{HCO}_3^-$  and  $\text{CO}_2$  ( $-5.5$ ‰), possibly, as a result of isotope fractionation during generation of methane from carbon dioxide.

Proceeding from the Le Chatelier principle, heat-releasing reactions are always directed toward maximum enthalpy decrease. Therefore, the generation of methane ( $\text{CH}_4$ ) from carbon dioxide with a mixture of  $^{12}\text{C}$  and  $^{13}\text{C}$  isotopes involves mainly  $^{12}\text{C}$  as its frac-

tionation releases 0.412 kcal/g [62]. This effect works toward lighter C isotope composition of the generated methane, and the reaction develops from left to right as



The  $\delta^{13}\text{C}$  values of methane in oceanic rifts are most often about  $-13$  or  $-14\%$ , while those of  $\text{HCO}_3^-$  and  $\text{CO}_2$  dissolved in seawater average about  $-5.5\%$  [20]. Therefore, the exchange reaction between carbon dioxide and methane develops toward lower  $\delta^{13}\text{C}$  of methane, according to (53). Later on,  $^{12}\text{C}$  in organic matter of microbial communities increases additionally as methane is consumed by bacteria, and  $\delta^{13}\text{C}_{\text{org}}$  reaches extremely low negative values of  $-50\%$  or even about  $-80\%$ . The same effect may account for the  $\delta^{13}\text{C}_{\text{org}}$  lows in methane of swamps and coalbeds.

## 6. Conclusions

Integrated data on the geodynamic evolution of the Arctic region and the chemical formation patterns of abiotic hydrocarbons have implications for the location of zones where such hydrocarbons are generated and released into the atmosphere and the hydrosphere, as well as for the origin, extent, and composition variations of hydrocarbon species.

Note that disseminated carbon in mafic igneous rocks has very low concentrations of 10 to 100 ppm and depleted  $\delta^{13}\text{C}$  values of  $-22$  to  $-27\%$ , while the average crustal isotope ratios are less negative ( $\delta^{13}\text{C} = -3$  to  $-8\%$ ) [83], and the isotopic shifts are similar to those in diamonds. Mid-ocean ridge basalts contain 20 to 170 ppm C with shifts of about  $-5\%$  [84]. The actual concentration of free carbon in the mantle must be still lower because some amount of carbon is bound as atoms in the structure of silicates [85] and some carbon participates in the crust–mantle cycle being entrained with mantle convective flows from subduction zones to rifts. Thus, the quantity of carbon in the mantle is vanishing and its total contents may be overestimated. Crustal carbonates store about  $3.91 \times 10^{23}$  g  $\text{CO}_2$  and  $1.95 \times 10^{22}$  g  $\text{C}_{\text{org}}$  [86]. A large part of this carbon is deposited as sediments on the seafloor or on continental slopes and is involved in the crust–mantle cycle and related convergent or divergent processes on plate boundaries.

Carbon species in rifts include diverse hydrocarbon gases from methane ( $\text{CH}_4$ ) and ethane ( $\text{C}_2\text{H}_6$ ) to propane ( $\text{C}_3\text{H}_8$ ) and butane ( $\text{C}_4\text{H}_{10}$ ) [59], but free higher hydrocarbons become unstable at high pressures and temperatures and tend to decompose into light species till  $\text{CH}_4$ . Therefore, C compounds originate at shallow depths in low-temperature conditions rather than being furnished from a deep mantle. Their diversity may be due to the fact that metal carbides remain stable under high pressures and temperatures in a dry mantle and dissociate only when reaching the hydration level of  $<400$  °C.

Isotope geochemical data show that hydrocarbon gases in rifts are compositionally diverse and C isotopes are subject to fractionation. The reason is that C-species generated in situ in rift zones coexist with genetically different carbon, with its particular isotope signatures, delivered by convective flows from subduction zones, which may bias the results of radiocarbon analysis yielding meaningless dates.

Thus, carbon involved in the crust–mantle cycle mostly originates in the shallow crust, becomes consumed in subduction zones, and is transported further to rifts. It undergoes multistage transformations from inorganic to organic species and back, sinks to the depths of mantle convection, and then rises through the rifted crust (Figure 1).

A large part of these generated abiotic hydrocarbon gases is released into the hydrosphere and atmosphere, and their amount in the lithosphere is too low to provide an accumulation of large oil or gas fields. However, some gases (mostly methane) may be buried in bottom sediments and form deposits of gas hydrates [24], which are climatically significant methane reservoirs with geological-scale characteristic times of evolution [7,8,87].

The revealed crust–mantle transport is a part of the global carbon cycle in which carbon migrates from the atmosphere to the mantle and back. The suggested mechanism of abiogenic methane production requires further studies in terms of the global carbon budget.

**Author Contributions:** Conceptualization, N.S. (Nickolay Sorokhtin) and L.L.; methodology, N.S. (Nickolay Sorokhtin) and L.L.; software, N.S. (Nickolay Sorokhtin); validation, N.S. (Nickolay Sorokhtin) and E.S.; formal analysis, N.S. (Nickolay Sorokhtin), L.L. and N.S. (Natalia Shakhova); investigation, N.S. (Nickolay Sorokhtin), L.L., N.S. (Natalia Shakhova) and I.S.; resources, L.L. and I.S.; data curation, N.S. (Nickolay Sorokhtin), E.S., N.K., R.A. and S.N.; writing—original draft preparation, N.S. (Nickolay Sorokhtin), L.L. and R.A.; writing—review and editing, all authors; visualization, N.S. (Nickolay Sorokhtin) and D.A.; supervision, L.L.; project administration, L.L. and I.S.; funding acquisition, I.S. All authors have read and agreed to the published version of the manuscript.

**Funding:** This study was carried out at the Tomsk State University as part of Program *Prioritet 2030* run by the Ministry of Science and Education of the Russian Federation. Regional application of the proposed mechanism of abiogenic methane origin in the ESAS was funded by the Russian Science Foundation (grant # 21-77-30001).

**Data Availability Statement:** Not applicable.

**Acknowledgments:** We appreciate reviewers' attention, comments, and advice aimed at improving this study.

**Conflicts of Interest:** The authors declare no conflict of interest.

## References

1. Koven, C.D.; Ringeval, B.; Friedlingstein, P.; Ciais, P.; Cadule, P.; Khvorostyanov, D.; Krinner, G.; Tarnocai, C. Permafrost carbon-climate feedbacks accelerate global warming. *Proc. Natl. Acad. Sci. USA* **2011**, *108*, 14769–14774. [[CrossRef](#)] [[PubMed](#)]
2. Friedlingstein, P.; Cox, P.; Betts, R.; Bopp, L.; Von Bloh, W.; Brovkin, V.; Cadule, P.; Doney, S.; Eby, M.; Fung, I.; et al. Climate–carbon cycle feedback analysis: Results from the C4MIP model intercomparison. *J. Clim.* **2006**, *19*, 3337–3353. [[CrossRef](#)]
3. Gruber, N. Warming up, turning sour, losing breath: Ocean biogeochemistry under global change. *Phil. Trans. R. Soc. A* **2011**, *369*, 1980–1996. [[CrossRef](#)] [[PubMed](#)]
4. Gramberg, I.S.; Kulakov, Y.N.; Pogrebitsky, Y.E.; Sorokov, D.S. Arctic Oil-Gas Superbasin. *Pet. Geol. A Dig. Russ. Lit. Pet. Geol.* **1985**, *22*, 158–161.
5. Lobkovskii, L.I.; Nikiforov, S.L.; Shakhova, N.E.; Semiletov, I.P.; Libina, N.V.; Anan'ev, R.A.; Dmitrevskii, N.N. Mechanisms responsible for degradation of submarine permafrost on the eastern Arctic shelf of Russia. *Dokl. Earth Sci.* **2013**, *449*, 280–283. [[CrossRef](#)]
6. Kvenvolden, K.A. Methane hydrates and global climate. *Glob. Biogeochem. Cycles* **1988**, *2*, 221–229. [[CrossRef](#)]
7. Shakhova, N.; Semiletov, I.; Chuvilin, E. Understanding the permafrost–hydrate system and associated methane releases in the East Siberian Arctic Shelf. *Geosciences* **2019**, *9*, 251. [[CrossRef](#)]
8. Shakhova, N.; Semiletov, I.; Leifer, I.; Rekant, P.; Salyuk, A.; Kosmach, D. Geochemical and geophysical evidence of methane release from the inner East Siberian Shelf. *J. Geophys. Res.* **2010**, *115*, C08007. [[CrossRef](#)]
9. Shakhova, N.; Semiletov, I.; Leifer, V.; Sergienko, A.; Salyuk, D.; Kosmach, D.; Chernikh, C.; Stubbs, D.; Nicolsky, V.; Tumskoy, O.; et al. Ebullition and storm-induced methane release from the East Siberian Arctic Shelf. *Nat. Geosci.* **2014**, *7*, 64–70. [[CrossRef](#)]
10. Steinbach, J.; Holmstrand, H.; Scherbakova, K.; Kosmach, D.; Bruchrt, V.; Shakhova, N.; Salyuk, A.; Sapart, C.; Chernikh, D.; Noormets, R.; et al. Source apportionment of methane escaping the subsea permafrost system in the outer Eurasian Arctic Shelf. *Proc. Natl. Acad. Sci. USA* **2021**, *118*, e2019672118. [[CrossRef](#)]
11. Cramer, B.; Franke, D. Indications for an Active Petroleum System in the Laptev Sea, NE Siberia. *J. Petrol. Geol.* **2005**, *28*, 369–384. [[CrossRef](#)]
12. Romanovskii, N.N.; Hubberten, H.-W.; Gavrillov, A.V.; Eliseeva, A.A.; Tipenko, G.S. Offshore permafrost and gas hydrate stability zone on the shelf of East Siberian Seas. *Geo-Marine Lett.* **2005**, *25*, 167–182. [[CrossRef](#)]
13. Shakhova, N.; Semiletov, I.; Salyuk, A.; Joussupov, V.; Kosmach, D.; Gustafsson, Ö. Extensive methane venting to the atmosphere from sediments of the East Siberian Arctic Shelf. *Science* **2010**, *327*, 1246–1250. [[CrossRef](#)]
14. Ruppel, C.D.; Kessler, J.D. The interaction of climate change and methane hydrates. *Rev. Geophys.* **2017**, *55*, 126–168. [[CrossRef](#)]
15. Sapart, C.J.; Shakhova, N.; Semiletov, I.; Jansen, J.; Szidat, S.; Kosmach, D.; Dudarev, O.; van der Veen, C.; Egger, M.; Sergienko, V.; et al. The origin of methane in the East Siberian Arctic Shelf unraveled with triple isotope analysis. *Biogeosciences* **2017**, *14*, 2283–2292. [[CrossRef](#)]
16. Fireman, E.L. Carbon-14 in lunar soil and in meteorites. In Proceedings of the Ninth Lunar and Planetary Science Conference, Houston, TX, USA, 13–17 March 1978; pp. 1647–1654.
17. Fireman, E.L.; Norris, T.L. Ages and composition of gas trapped in Allan Hills and Byrd core ice. *Earth Planet. Sci. Lett.* **1982**, *60*, 339–350. [[CrossRef](#)]
18. Baudin, G.; Blain, C.; Hagemann, R.; Kremer, M.; Lucas, M.; Merlivat, L.; Molina, R.; Nieff, G.; Prost Marechal, P.; Regnaud, F.; et al. Quelques données nouvelles sur les réactions nucléaires en chaîne qui se sont produites dans le gisement d'Oklo, C.R. *Acad. Sci. Paris* **1973**, *275D*, 2291. (In French)

19. Dmitriev, L.V.; Bazylev, B.A.; Silantiev, S.A.; Borisov, M.V.; Sokolov, S.Y.; Bugo, A. Hydrogen and methane formation with serpentization of mantle hyperbasite of the ocean and oil generation. *Russ. J. Earth Sci.* **1999**, *1*, 511–519. [[CrossRef](#)]
20. Sorokhtin, O.G.; Lein, A.Y.; Balanyuk, I.E. Thermodynamics of oceanic hydrothermal systems and abiogenic methane generation. *Oceanology* **2001**, *41*, 861–872.
21. Sorokhtin, O.G.; Chilingarian, G.V.; Sorokhtin, N.O. Evolution of Earth and its Climate: Birth, Life and Death of Earth. In *Developments in Earth and Environmental Sciences*, 1st ed.; Elsevier: Amsterdam, The Netherlands, 2011; Volume 10, p. 763.
22. Sorokhtin, N.O.; Lobkovsky, L.I.; Semiletov, I.P. Carbon depth cycle and formation of abiogenic hydrocarbons. *Bull. Tomsk Polytech. Univ. Eng. Georesources* **2018**, *329*, 156–173. (In Russian)
23. Sorokhtin, N.O.; Lobkovsky, L.I.; Kozlov, N.E. The crust-mantle carbon cycle and origin of abiogenic hydrocarbons. *Oceanology* **2020**, *60*, 248–258. [[CrossRef](#)]
24. Dmitrievsky, A.N.; Balanyuk, I.E.; Matveenkov, V.V.; Sorokhtin, O.G. Modern views on the possibility of hydrocarbon generation with the participation of oceanic crust rocks. *Dokl. Earth Sci.* **2000**, *371*, 385–387.
25. Dmitrievsky, A.N.; Balanyuk, I.E. *Gas Hydrates of Seas and Oceans—A Hydrocarbon Source of the Future*; IRTs Gazprom Ltd.: Moscow, Russia, 2009; p. 416.
26. Lein, A.Y.; Peresyupkin, V.I.; Simoneit, B.R.T. Origin of hydrocarbons in hydrothermal sulfide ores in the Mid-Atlantic Ridge. *Lithol. Miner. Resour.* **2003**, *38*, 383–393. [[CrossRef](#)]
27. Uspensky, V.A. *Carbon Budget in the Biosphere: Implications for Carbon Distribution in the Crust*; VNIGRI, Gostoptehizdat: Leningrad, Russia, 1956; p. 101. (In Russian)
28. Varotsos, C.A.; Krapivin, V.F.; Soldatov, V.Y. Modeling the carbon and nitrogen cycles. *Front. Environ. Sci.* **2014**, *2*, 8. [[CrossRef](#)]
29. Romankevich, E.A.; Vetrov, A.A. Masses of carbon in the Earth's hydrosphere. *Geochem. Int.* **2013**, *51*, 431–455. [[CrossRef](#)]
30. Krapivin, V.F.; Varotsos, C.A. *Biogeochemical Cycles in Globalization and Sustainable Development*; Springer/Praxis: Chichester, UK, 2008; p. 562.
31. Galimov, E.M. *Carbon Isotopes in Oil and Gas Geology*; NASA TT F-682; National Aeronautics and Space Administration: Washington, DC, USA, 1975; p. 395.
32. Dobretsov, N.L.; Shatskiy, A.F. Deep carbon cycle and geodynamics: The role of the core and carbonatite melts in the lower mantle. *Russ. Geol. Geophys.* **2012**, *53*, 1117–1132. [[CrossRef](#)]
33. Dobretsov, N.L.; Koulakov, I.; Kukarina, E.V.; Litasov, K.D. An integrate model of subduction: Contributions from geology, experimental petrology, and seismic tomography. *Russ. Geol. Geophys.* **2015**, *56*, 13–38. [[CrossRef](#)]
34. Sobolev, N.V.; Dobretsov, N.L.; Ohtani, E.; Taylor, L.A.; Schertl, H.-P.; Palyanov, Y.N.; Litasov, K.D. Problems related to crystallogenesis and the deep carbon cycle. *Russ. Geol. Geophys.* **2015**, *56*, 1–12. [[CrossRef](#)]
35. Lobkovsky, L.I. Deformable plate tectonics and regional geodynamic model of the Arctic region and Northeastern Asia. *Russ. Geol. Geophys.* **2016**, *57*, 371–386. [[CrossRef](#)]
36. Kazmin, Y.B.; Lobkovskii, L.I.; Kononov, M.V. The geodynamic model of Cretaceous-Cenozoic evolution of the Arctic Basin. *Dokl. Earth Sci.* **2015**, *462*, 559–564. [[CrossRef](#)]
37. Lobkovsky, L.I.; Garagash, I.A.; Kononov, M.V.; Verzhbitsky, V.E.; Kotelkin, V.D. Tectonics of deformable plates and the Mesozoic-Cenozoic geodynamic history of the Arctic region. In *Geology and Geoenvironment of Eurasian Continental Margins*; GEOS: Moscow, Russia, 2010; pp. 8–40. (In Russian)
38. Lobkovsky, L.I.; Alekseev, D.A.; Garagash, I.A. Geodynamic evolution model of the major structures of Amerasian Basin. *Dokl. Earth Sci.* **2018**, *480*, 753–757. [[CrossRef](#)]
39. Laverov, N.P.; Lobkovsky, L.I.; Kononov, M.V.; Dobretsov, N.L.; Vernikovskiy, V.A.; Sokolov, S.D.; Shipilov, E.V. A geodynamic model of the evolution of the Arctic basin and adjacent territories in the Mesozoic and Cenozoic and the outer limit of the Russian Continental Shelf. *Geotectonics* **2013**, *354*, 1–30. [[CrossRef](#)]
40. Shipilov, E.V.; Lobkovsky, L.I. Tectono-geodynamic transformations of the Amerasian Basin lithosphere in the Cenozoic. *Dokl. Earth Sci.* **2012**, *445*, 979–985. [[CrossRef](#)]
41. Lobkovsky, L.I.; Shipilov, E.V.; Kononov, M.V. Geodynamic model of upper mantle convection and transformation of the Arctic lithosphere in the Mesozoic and Cenozoic. *Izvestiya. Phys. Solid Earth* **2013**, *49*, 767–785. [[CrossRef](#)]
42. Shipilov, E.V.; Lobkovsky, L.I.; Shkarubo, S.I. Structure of the Khatanga–Lomonosov fracture zone according to seismic data. *Dokl. Earth Sci.* **2019**, *487*, 846–851. [[CrossRef](#)]
43. Zhao, D. Multiscale seismic tomography and mantle dynamics. *Gondwana Res.* **2009**, *15*, 297–323. [[CrossRef](#)]
44. Zhao, D.; Tian, Y.; Ley, J.; Liu, L.; Zheng, S. Seismic image and origin of the Changbai intraplate volcano in East Asia: Role of big mantle wedge above the stagnant Pacific slab. *Phys. Earth Planet. Int.* **2009**, *173*, 197–206. [[CrossRef](#)]
45. Zhao, D.; Pirajno, F.; Liu, L. Mantle structure and dynamics under East Russia and adjacent regions. *Russ. Geol. Geophys.* **2010**, *51*, 925–938. [[CrossRef](#)]
46. Lobkovsky, L.I.; Nikishin, A.I.; Khain, V.I. *Modern Problems of Tectonics and Geodynamics*; Nauchnyi Mir: Moscow, Russia, 2004; p. 612. (In Russian)
47. Sorokhtin, N.O. *The Origins of Natural Diamonds*; Scrivener Publishing Wiley: Beverly, MA, USA, 2019; p. 532.
48. Miller, E.L.; Verzhbitsky, V.E. Structural studies near Pevek, Russia: Implications for formation of the East Siberian Shelf and Makarov Basin of the Arctic Ocean. In *Geology, Geophysics and Tectonics of Northeastern Russia: A Tribute to Leonid Parfenov*;

- Stone, D.B.; Fujita, K.; Layer, P.W.; Miller, E.L.; Prokopiev, A.V.; Toro, J., Eds.; EGU Stephan Mueller Publication Series: Munich, Germany, 2009; Volume 4, pp. 223–241.
49. Shipilov, E.V. Generations, stages, and specifics of geodynamic evolution of young ocean formation in the Arctic. *Dokl. Earth Sci.* **2005**, *402*, 529–533.
50. Shipilov, E.V. Tectono-geodynamic evolution of Arctic continental margins during epochs of young ocean formation. *Geotectonics* **2004**, *38*, 343–365.
51. Shipilov, E.V. Generations of spreading basins and stages of breakdown of Wegener’s Pangea in the geodynamic evolution of the Arctic Ocean. *Geotectonics* **2008**, *42*, 105–124. [[CrossRef](#)]
52. Chernykh, A.; Glebovsky, V.; Zykov, M.; Korneva, M. New insights into tectonics and evolution of the Amerasia Basin. *J. Geodyn.* **2018**, *119*, 167–182. [[CrossRef](#)]
53. Faleide, J.I.; Tsikalas, F.; Eldholm, O. Evolution of conjugate continental margin in a regional rift-shear tectonic setting: The Lofoten-SW Barents Sea and NE Greenland margin in the NE Atlantic. In *Arctic Geology, Hydrocarbon Resources and Environmental Challenges*; Smelror, M., Bugge, T., Eds.; Norsk Geologisk Forening (NGF): Tromsø, Norway, 2004; Volume 2, pp. 45–46.
54. Piepjohn, K.; Lorenz, H.; Franke, F.; Brandes, C.; von Gosen, W.; Gaedicke, C.; Labrousse, L.; Sobolev, N.; Sobolev, P.; Suan, G.; et al. Mesozoic structural evolution of the New Siberian Islands. Project Circum-Arctic Lithosphere Evolution (CASE). *Geol. Soc. Lond. Spec. Publ.* **2018**, *460*, 239–262. [[CrossRef](#)]
55. Drachev, S.S.; Shkarubo, S.I. Tectonics of the Laptev Shelf, Siberian Arctic. Project Circum-Arctic Lithosphere Evolution (CASE). *Geol. Soc. Lond. Spec. Publ.* **2017**, *460*, 263–284. [[CrossRef](#)]
56. Drachev, S.S.; Mazur, S.; Campbel, S.; Green, C. Crustal architecture of the East Siberian Arctic Shelf and adjacent Arctic Ocean constrained by seismic data and gravity modeling results. *J. Geodyn.* **2018**, *119*, 123–148. [[CrossRef](#)]
57. Gurvich, E.G. *Metalliferous Sediments of the World Ocean: Fundamental Theory of Deep-Sea Hydrothermal Sedimentation*; Springer: Berlin/Heidelberg, Germany, 2006; p. 416.
58. Lein, A.Y.; Bogdanov, Y.A.; Lisitzin, A.P. Processes of hydrothermal ore genesis in the World Ocean: The results of 35 years of research. *Dokl. Earth Sci.* **2016**, *466*, 38–41. [[CrossRef](#)]
59. Cruse, A.M.; Seewald, J.S. Chemistry of low-molecular weight hydrothermal fluids from Middle Valley, Northern Juan de Fuca Ridge. *Geochim. Cosmochim. Acta* **2006**, *70*, 2079–2092. [[CrossRef](#)]
60. Proskurowski, G.; Lilley, M.D.; Seewald, J.S.; Früh-Green, G.L.; Olson, E.J.; Lupton, J.E.; Sylva, S.P.; Kelley, D.S. Abiogenic hydrocarbon production at Lost City hydrothermal field. *Science* **2008**, *319*, 604–607. [[CrossRef](#)] [[PubMed](#)]
61. Kosolapova, T.Y. *Carbides: Properties, Production, and Applications*; Plenum Press: New York, NY, USA, 1971; p. 298.
62. Sorokhtin, O.G.; Mitrofanov, F.P.; Sorokhtin, N.O. *Origin of Diamonds and Diamond Potential of the Eastern Fennoscandian Shield*; KSC: Apatity, Russia, 1996; p. 144. (In Russian)
63. Zharikov, V.A.; Shmulovich, K.I.; Bulatov, V.K. Experimental studies in the system CaO-MgO-Al<sub>2</sub>O<sub>3</sub>—SiO<sub>2</sub>-CO<sub>2</sub>—H<sub>2</sub>O and conditions of high-temperature metamorphism. *Tectonophysics* **1977**, *43*, 145–162. [[CrossRef](#)]
64. Cooper, B.S.; Coleman, S.H.; Barnard, P.C.; Butterworth, J.S. Paleotemperatures in the northern North Sea Basin. *Petrol. and Cont. Shelf North-West Europe. Geology* **1975**, *1*, 487–492.
65. Sobolev, N.V. *Deep-Seated Inclusions in Kimberlites and the Problem of the Composition of the Upper Mantle*; American Geological Union: Washington, DC, USA, 1977; p. 279.
66. Ringwood, A.E.; Major, A. The system Mg<sub>2</sub>SiO<sub>4</sub>—Fe<sub>2</sub>SiO<sub>4</sub> at high pressures and temperatures. *Phys. Earth Planet. Inter.* **1970**, *3*, 89–108. [[CrossRef](#)]
67. Dawson, J.B. *Kimberlites and Their Xenoliths*; Springer: Heidelberg, Germany, 1980; p. 252.
68. Kennedy, C.S.; Kennedy, G.C. The equilibrium boundary between graphite and diamond. *J. Geophys. Res.* **1976**, *81*, 2467–2470. [[CrossRef](#)]
69. Bucher, K.; Frey, M. *Petrogenesis of Metamorphic Rock*, 7th ed.; Springer: Heidelberg, Germany, 2022; p. 341.
70. Karrer, P. *Lehrbuch der Organischen Chemie*; Thieme: Stuttgart, Germany, 1959; p. 1216. (In German)
71. Sorokhtin, O.G. Plate Tectonics and Origin of Diamondiferous Kimberlites. In *General and Regional Geology*; VIEMS: Moscow, Russia, 1985; p. 47. (In Russian)
72. Sorokhtin, O.G.; Chilingar, G.V.; Khilyuk, L.F. Global Warming and Global Cooling: Evolution of Climate on Earth. In *Developments in Earth and Environmental Sciences*, 1st ed.; Elsevier: Amsterdam, The Netherlands, 2011; Volume 5, p. 323.
73. Naumov, G.B.; Ryzhenko, B.N.; Khodakovskiy, I.L. *Handbook of Thermodynamic Data*; US Geological Survey, Water Resources Division: Menlo Park, CA, USA, 1974; Volume 226, p. 328.
74. Kenney, J.F.; Kutcherov, V.A.; Bendeliani, N.A.; Alekseev, V.A. The evolution of multicomponent system at high pressures: VI. The thermodynamic stability of the hydrogen–carbon system: The genesis of hydrocarbons and the origin of petroleum. *Proc. Natl. Acad. Sci. USA* **2002**, *99*, 10976–10981. [[CrossRef](#)] [[PubMed](#)]
75. Kutcherov, V.A.; Bendeliani, N.A.; Alekseev, V.A.; Kenney, J.F. Synthesis of hydrocarbons from minerals at pressures up to 5 GPa. *Dokl. Phys. Chem.* **2002**, *387*, 328–330. [[CrossRef](#)]
76. Melton, C.E.; Giardini, A.A. The composition and significance of gas released from natural diamonds from Africa and Brazil. *Amer. Miner.* **1974**, *59*, 775–782.
77. Agte, C.; Moers, K. Über innerkomplexe Brenzcatechinate vierwertiger Elemente. *Z. Für Anorg. Und Allg. Chemie.* **1931**, *B198*, 233. (In German) [[CrossRef](#)]

78. *Refractory Carbides*; Samsonov, G.V. (Ed.) Springer: New York, NY, USA, 1970; p. 461.
79. Campbell, I.E.; Powell, C.F.; Nowicki, D.H.; Gonser, B.W. The vapor-phase deposition of refractory materials: I. General conditions and apparatus. *Electrochem. Soc.* **1949**, *96*, 318–333. [[CrossRef](#)]
80. Hoefs, J. *Stable Isotope Geochemistry*; Springer: Berlin/Heidelberg, Germany, 2009; p. 286.
81. Swart, P.K.; Pillinger, C.T.; Milledge, H.J.; Seal, M. Carbon isotopic variation within individual diamonds. *Nature* **1983**, *303*, 793–795. [[CrossRef](#)]
82. Galimov, E.M. Isotope fractionation related to kimberlite magmatism and diamond formation. *Geochim. Cosmochim. Acta* **1991**, *55*, 1697–1708. [[CrossRef](#)]
83. Galimov, E.M. Origin and evolution of oceans: Evidence from  $^{18}\text{O}/^{16}\text{O}$  changes in sediments through geological time. *Dokl. AN SSSR* **1988**, *299*, 977–981. (In Russian)
84. Exley, R.A.; Matthey, D.P.; Clague, D.A.; Pillinger, C.T. Carbon isotope systematic of a mantle “hotspot”: A comparison of Loihi Seamount and MORB glasses. *Earth Planet. Sci. Lett.* **1986**, *78*, 189–199. [[CrossRef](#)]
85. Watanabe, S.; Mishima, K.; Matsuo, S. Isotopic ratios of carbonaceous materials incorporated in olivine crystals from the Hualalai volcano Hawaii. An approach to mantle carbon. *Geochim. J.* **1983**, *17*, 95–104. [[CrossRef](#)]
86. Ronov, A.B.; Yaroshevskiy, A.A.; Migdisov, A.A. Chemical constitution of the Earth’s crust and geochemical balance of the major elements. *Int. Geol. Rev.* **1991**, *33*, 941–1048. [[CrossRef](#)]
87. Shakhova, N.; Semiletov, I.; Gustafsson, Ö.; Sergienko, V.; Lobkovsky, L.; Dudarev, O.; Tumskey, T.; Grigoriev, M.; Mazurov, A.; Salyuk, A.; et al. Current rates and mechanisms of subsea permafrost degradation in the East Siberian Arctic Shelf. *Nat. Commun.* **2017**, *8*, 15872. [[CrossRef](#)] [[PubMed](#)]

**Disclaimer/Publisher’s Note:** The statements, opinions and data contained in all publications are solely those of the individual author(s) and contributor(s) and not of MDPI and/or the editor(s). MDPI and/or the editor(s) disclaim responsibility for any injury to people or property resulting from any ideas, methods, instructions or products referred to in the content.